Available online at www.sciencedirect.com
SCIENCE DIRECT®
International Journal of Heat and Mass Transfer 48 (2005) 1518–1533
International Journal of HEAT and MASS TRANSFER
www.elsevier.com/locate/ijhmt

An experimental investigation of microchannel flow with internal pressure measurements

M.J. Kohl, S.I. Abdel-Khalik *, S.M. Jeter, D.L. Sadowski

George Woodruff School of Mechanical Engineering, Georgia Institute of Technology, Atlanta, GA 30332-0405, USA

Received 4 May 2004; received in revised form 13 October 2004
Available online 22 December 2004

Abstract

Experiments have been conducted to investigate discrepancies in previously published data for the pressure drop in microchannels. Straight channel test sections with integrated pressure sensors were developed with channel hydraulic diameters ranging from 25 to 100 μm. Compressible flow results for $6.8 < Re < 18{,}814$ and incompressible flow results for $4.9 < Re < 2068$ have been obtained. The results suggest that friction factors for microchannels can be accurately determined from data for standard large channels. The large inconsistencies in previously published data are probably due to instrumentation errors and/or improper accounting for compressibility effects.

Keywords: Microchannel; Microfluidics; Compressible; Pressure sensor

1. Introduction

In recent years, the proliferation of MEMS and microfluidic devices has resulted in the use of microchannels in many applications. Because of the wide range of uses for microchannels, it is important to be able to predict their behavior both thermally and hydrodynamicly. According to conventional theory, continuum based models for channels should apply as long as the Knudsen number, *Kn*, is lower than 0.01 where *Kn* is the ratio of the mean free path for the fluid, λ, to an appropriate geometric length scale. For air at atmospheric pressure, *Kn* is typically lower than 0.01 for channels with hydraulic diameters greater than 7 μm. Contrary to this prediction, experimental investigations of microchannel flow have found discrepancies between standard models and microchannel flow measurements.

Since Tuckerman and Pease [1] developed the first microchannel water-cooled heat sink, many researchers have proceeded to study flow and heat transfer in microchannels in greater detail. Because most applications for microfluidics deal with liquids, most of the past research has focused on microchannel liquid flows. Several studies on low Reynolds number ($Re < 100$) flows of water have been reported. Wilding et al. [2] measured friction factors that were approximately 1.3 times greater than predicted. Papautsky et al. [3] reported an approximate 20% increase in the normalized friction factors obtained during the experiment. Jiang et al. [4] found that measured friction factors were between 1.15 and 1.75 times greater than predicted, with the shorter channels showing the greatest increase. However, due to the low

* Corresponding author. Tel.: +1 404 894 3719; fax: +1 404 894 8496.
E-mail address: said.abdelkhalik@me.gatech.edu (S.I. Abdel-Khalik).

0017-9310/$ - see front matter © 2004 Elsevier Ltd. All rights reserved.
doi:10.1016/j.ijheatmasstransfer.2004.10.030

Nomenclature

A	cross sectional are of channel, m^2
D_h	hydraulic diameter, m
f_{exp}	measured friction factor
f_{th}	theoretical friction factor
$(fRe)_{inc}$	analytical (fRe) for laminar incompressible flow [6]
h	channel height, m
K_L	minor loss coefficient
K_∞	developing flow loss coefficient
Kn	Knudsen number, λ/l
L	channel length, m
M	Mach number
m	mass, kg
$\dot{m}$	mass flow rate, kg/s
Nu	Nusselt number
p	pressure, Pa
$p_{c,in}$	pressure at channel inlet, Pa
$p_{c,out}$	pressure at channel exit, Pa
p_v	gas pressure for volumetric flow rate measurement, Pa
R	ideal gas constant, J/kg K
R_a	average surface roughness, m
Re	Reynolds number, $\rho D_{h\ u}/\mu$
Re_c	critical Reynolds number
T	temperature, K
T_v	temperature measurement for volumetric flow rate measurement, K
u	average cross-sectional velocity, m/s
V	volume, m^3
w	channel width, m
γ	ratio of specific heats
μ	viscosity, N s/m^2
ρ	density, kg/m^3
Δp_{dev}	Δp associated with the developing flow, Pa
Δp_{ext}	Δp between pressure transducers and brace, Pa
$\Delta p_{loss,n}$	minor loss associated with geometry n, Pa
Δt	time measurement, s

L/D_h for the channels tested by Jiang, the increase in f may have been due to the fact that entrance effects were not appropriately accounted for.

Other researchers have investigated larger Re flows of water in microchannels. Mala and Li [5] obtained friction factors that were greater than those predicted by Shah and London [6] for channel hydraulic diameters less then 152 μm, and, as the diameter of the tubes decreased, the deviation of the friction factor measurements from theory increased. A follow up study by Weilin et al. [7] obtained results similar to those of Mala and Li with friction factors being greater than those predicted by Shah and London [6]. Wu and Cheng [8] found that their results matched the predictions of the analytical expression obtained by Ma and Peterson [9] to within ±11%. Experiments conducted by Sharp and Adrian [10], measured liquid pressure drops that agreed with Poiseulle flow predictions and by using micro-PIV they were able to observe that transition to turbulence was initiated between 1800 and 2000.

Previous research has also explored gas flows in microchannels. Wu and Little [11] experimented with channels having hydraulic diameters from 45 to 83 μm. Their measured friction factors for laminar flow were much greater than the analytical predictions of Shah and London [6]. Turbulent flow results were slightly greater than predicted by the Blasius equation [12]. They ascribed the differences to the increased relative roughness of the microchannels. It was also reported that the transition from laminar to turbulent flow occurred much earlier than expected and as early as $Re \approx 400$. Pfahler et al. [13,14] tested liquids and gases and found that the friction factor results were less than those predicted by Shah and London [6] and noted that friction factors decreased with decreasing channel depths. Harley et al. [15] found that their measurements had good agreement with predictions based on Shah and London [6], with f_{exp}/f_{th} ranging from 0.98 to 1.03 for $5 < Re < 1200$. Chung et al. [16] tested water and N_2 gas and found that their results for water matched the predictions of Shah and London [6] and the N_2 results were found to be well correlated to standard theory as long as compressibility effects were taken into account. Analytical and experimental work conducted by Arklic et al. [17] showed that by accounting for compressibility of gaseous flows, the measured results agreed with Navier–Stokes predictions.

In addition to microchannel pressure drops, some research has also explored heat transfer in microchannels. Choi et al. [18] examined both the flow and heat transfer properties of microchannel flows. During laminar flow, the measured friction factors were both above and below predictions based on Shah and London [6] and the Nusselt number, Nu, was found to have a Re dependence, contrary to the expected constant for fully-developed laminar flow in circular channels with constant wall temperature ($Nu = 3.66$). For turbulent flow, Choi et al. found that the friction factors were consistently less than those predicted by the Blasius equation and that the heat transfer results were found to be greater than those

predicted by the Dittus–Boelter equation [19]. Yu et al. [20] measured friction factors that were below standard predictions for both laminar and turbulent flow. Turbulent convection was found to be greater than predicted by the Dittus–Boelter equation [19] but less than the results of Choi et al. Hegab et al. [21] found that while laminar data was in agreement with standard analytical models, transitional and turbulent flow pressure drops were found to be lower than expected. Heat transfer rates were found to be lower than expected for all flow regimes.

Friction factors measured by Peng et al. [22–24] for laminar flow were found to be as much as 10 times greater than those predicted by Shah and London [6]. The measured friction factors in turbulent flow were between 4 and 0.1 times as great as predictions obtained using the Blasius equation. Convection results for turbulent flow were found to be both above and below the values predicted by the Dittus–Boelter equation [19], depending more on the channel geometry than the Reynolds number. Peng et al. also reported that the transition from laminar to turbulent flow occurred at Reynolds numbers of 200–700.

From the above descriptions of past research it is clear that there is a great amount of variation in the results that have been obtained. To help illustrate the range of experiments and results, the experiments discussed above have been summarized into Fig. 1, which summarizes microchannel flow data for liquids and Fig. 2, which summarizes data for gases. The data presented in these figures was scaled off from plots presented in the referenced papers. Figs. 1 and 2 display the friction factor data normalized with respect to the theoretical friction factor, f_{exp}/f_{th}. For laminar flow the theoretical friction factors were taken to be the geometry dependent values from Shah and London [6]. For a circular cross section this is the familiar $f = 64/Re$. For the sake of comparison it was assumed that laminar flow was maintained in all experiments for Re up to 2300, even though there may have been reported evidence of "early flow transition". For turbulent flow, the Blasius relation was used as the theoretical comparison.

Prior to the current investigation, it was not clear whether the differences between measured and predicted values were the result of some yet to be determined phenomenon, or due to errors and uncertainties in the reported data. It is important to note that when the data from a given paper is examined independently, it often shows a consistent deviation from the standard predictions. However, when the data from many papers are summarized, as shown in Figs. 1 and 2, the data are randomly scattered both above and below the standard predictions for large channels. This global view of the previous data may signify "better agreement" between measurements and theory than previously expected.

The instrumentation of all experiments discussed above is relatively similar. Due to limitations associated with the small size of the channels, pressures and temperatures were not measured directly inside the microchannels. To obtain the channel entrance and exit

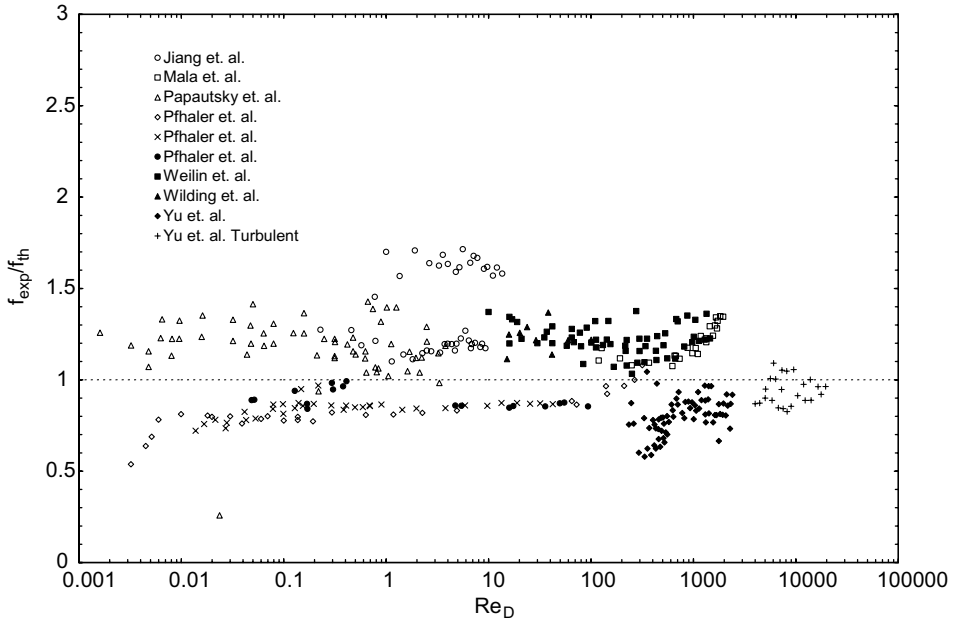

Fig. 1. Experimental friction factor data for liquids, f_{exp}, normalized by the theoretical value, f_{th}, based on Shah and London [6].

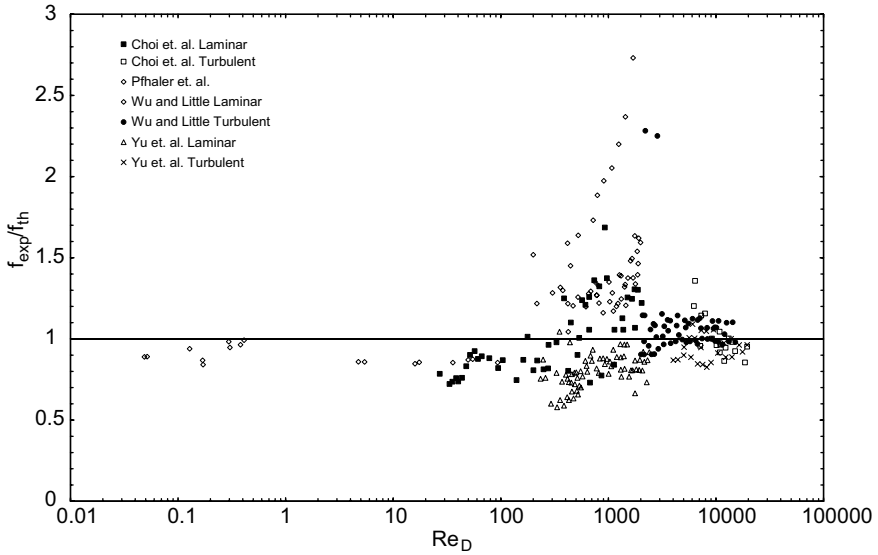

Fig. 2. Experimental friction factor data for gases, f_{exp}, normalized by the theoretical value, f_{th}, based on Shah and London [6].

pressures, measurements were taken in a plenum or supply line prior to entering the channel. A loss coefficient was sometimes assumed to account for entrance and exit losses. Additionally, losses must be considered for any piping between the channel plenums and the pressure transducers.

One method for improving the measurement of friction factors in microchannels would be to obtain pressure measurements inside the channel itself in order to eliminate the assumptions required by previously used methods. Experiments have been developed that integrate pressure sensors with a microchannel, allowing the static pressure inside the channel to be measured at multiple locations. Unfortunately these previous experiments have consisted of either surface micromachined channels with channel heights on the order of 1–2 μm [25–27] or of channels that are conventionally machined and are typically larger than $D_h = 250$ μm [28]. Due to the difficulty of getting integrated sensors to operate properly and the limited range of channel dimensions tested, previous sensor integrated experiments have provided little additional information about microchannel flows when $Kn < 0.01$.

The primary goal of the current investigation is to determine the validity of the standard continuum based models for microchannel flows where $Kn < 0.01$. Additionally, the results are used to identify possible causes for the scatter of friction factor data and observations of decreased critical Reynolds numbers. The experiment was designed to investigate pressure drop in microchannels and enables the measurement of pressures along the channel length for channel dimensions for which no internal pressure data are currently available.

2. Experimental apparatus and procedure

In order to improve on previous research it was necessary to construct microchannels in such a way that internal pressure measurements could be made. This was done by integrating tap lines and pressure sensing membranes into a system of silicon chips using microfabrication technologies. The microchannel system consists of three silicon chips (Fig. 3). The lower chip contains the microchannel test section with inlet and exit plenums and static pressure tap lines. The microchannel was fabricated by etching ⟨1 1 0⟩ silicon wafers in KOH, resulting in channels with a rectangular cross-section. Eight tap lines intersect the microchannel at equally spaced intervals and one tap line per plenum is also included. The tap line to microchannel intersection was etched by a deep silicon RIE process that resulted in tap line intersections with a width less then 7 μm and typical depths on the order of 10 μm. The middle chip is used to seal the channel and tap lines and provides ports for introducing and removing fluid from the channel plenums. Ten ports are also included in the middle chip to connect the tap lines to the pressure membrane chip, which is located on the top. The pressure membrane chip contains 10 rectangular membranes for sensing pressure from the tap lines. The membranes are KOH etched out of ⟨1 0 0⟩ silicon wafers and are approximately 0.564 mm wide, 10 mm long and 50 μm thick. Fig. 4 is a schematic of the fluid filled volume of the microchannel and system including the tap lines and pressure sensor volumes.

Table 1 summarizes the average geometry measurements for the channels used in the experiments.

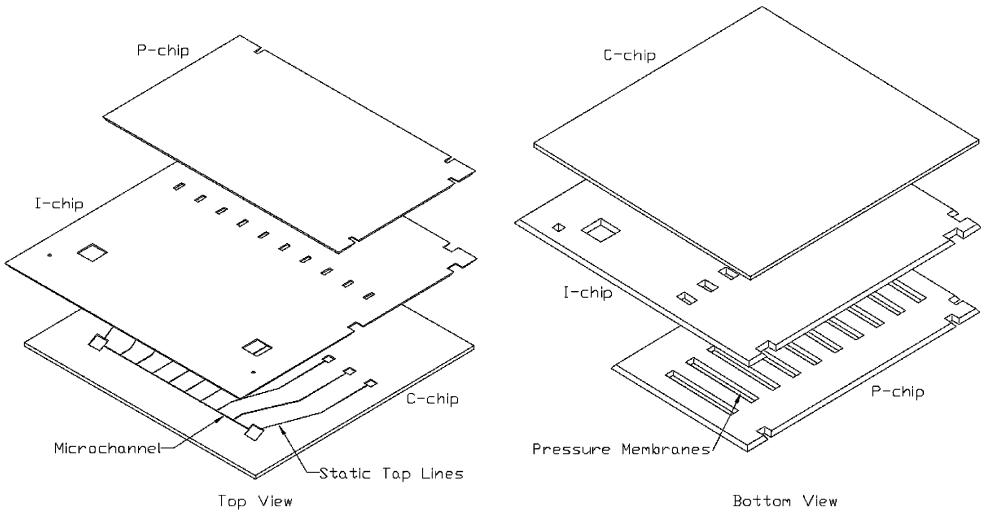

Fig. 3. Microfabricated test-section components, exploded top and bottom views.

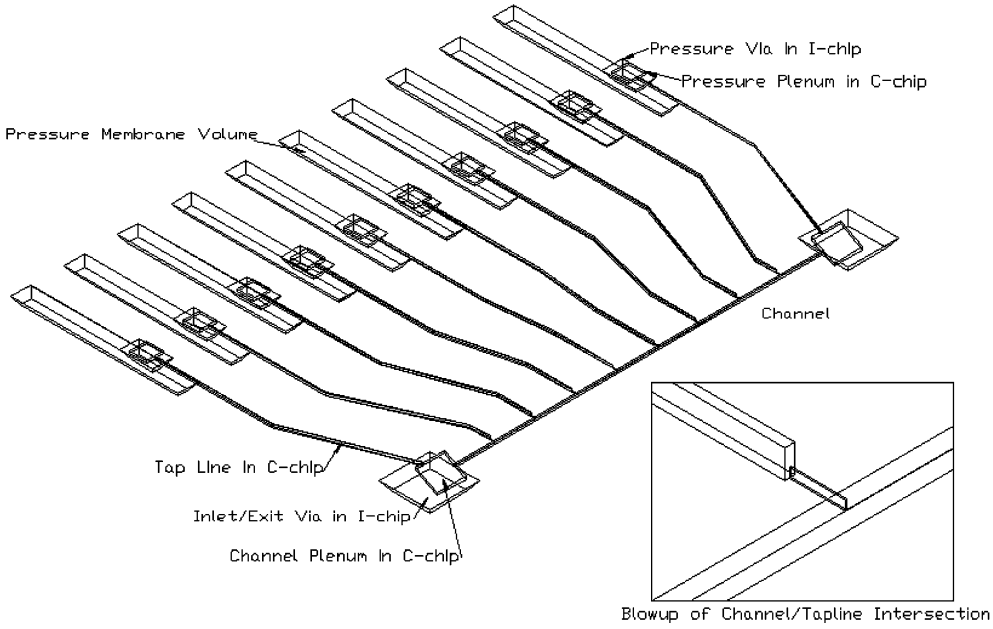

Fig. 4. Fluid filled volume of the microchannel system showing the connections between the microchannel, static tap lines and the fluid filled volume of the pressure sensors.

Table 1
Summary of the dimensions of channels used in the experiments

Channel	h (μm)	w (μm)	D_h (μm)	L/D_h	$(fRe)_{inc}$	R_a (μm)	Re_{max} (air)	Re_{max} (water)
a	24.2 ± 0.1	25.6 ± 0.1	24.9	401.9	56.93	0.33	5319.2	114.4
b	25.9 ± 0.1	101.1 ± 0.2	41.2	533.6	72.56	0.38	5983.2	210.6
c	43.6 ± 0.1	101.0 ± 0.2	60.9	361.1	64.30	0.33	10521.7	–
d	85.6 ± 0.2	101.8 ± 0.2	93.0	236.6	57.28	0.27	16732.3	1643.4
e	98.4 ± 0.2	101.3 ± 0.2	99.8	220.4	56.91	0.47	18814.3	2067.7

The measurements were obtained by a Wyko optical profilometer, which has a reported resolution of 3 nm. Also summarized in Table 1 are the maximum *Re* evaluated for each channel, the average surface roughness, R_a, and the standard incompressible theory predictions for *fRe*. It should be noted that all tests were for $Kn < 0.01$.

The three-chip system is held together by a brace that connects the microchannel to an external fluid handling system. The retaining force of the brace seals the individual microcomponents. The brace has a slot machined into it so that the deflection of the pressure membranes can be optically observed. An external system is used to supply the test fluid to the brace. Since experiments were run with both air and water, the fluid handling system had to be modified in order to address the specific issues associated with each. The fluid handling setup for the experiments is shown in Fig. 5.

The test fluid used for all gas experiments is air. A gas cylinder and a pressure regulator capable of regulating pressures up to 500 psig are used to supply the air.

The major difference between the gas and liquid handling systems is the addition of the, hydraulic cylinder, brass tank, and the water preparation system. The hydraulic cylinder is used to provide a constant pressure and flow of water to the inlet of the microchannel. One side of the cylinder is pressurized with regulated air from a tank while the other side is filled with water. Water in the brass tank is pressurized by the hydraulic cylinder and is passed into the same system used for the gas experiments. Before water is used in the experiment it is either saturated with air or degassed. The setup for degassing the water is shown in the lower part of Fig. 5. Water is degassed before being introduced to the system through valve 7, which is closed during the experiments.

Pressure and temperature measurements are made of the test fluid both upstream and downstream of the brace. The pressure sensors were calibrated and the uncertainty of the calibrations were ±0.2 psi for the inlet transducer and ±0.7 psi for the exit transducer. The inlet and exit temperatures are measured by 1/16-inch type T thermocouple probes. The calibration uncertainties were ±0.07 °C for the inlet temperature and ±0.2 °C for the exit temperature.

The valves on the system can be adjusted to either pressurize the entire system for pressure sensor calibration or to direct all fluid through the microchannel during experiments.

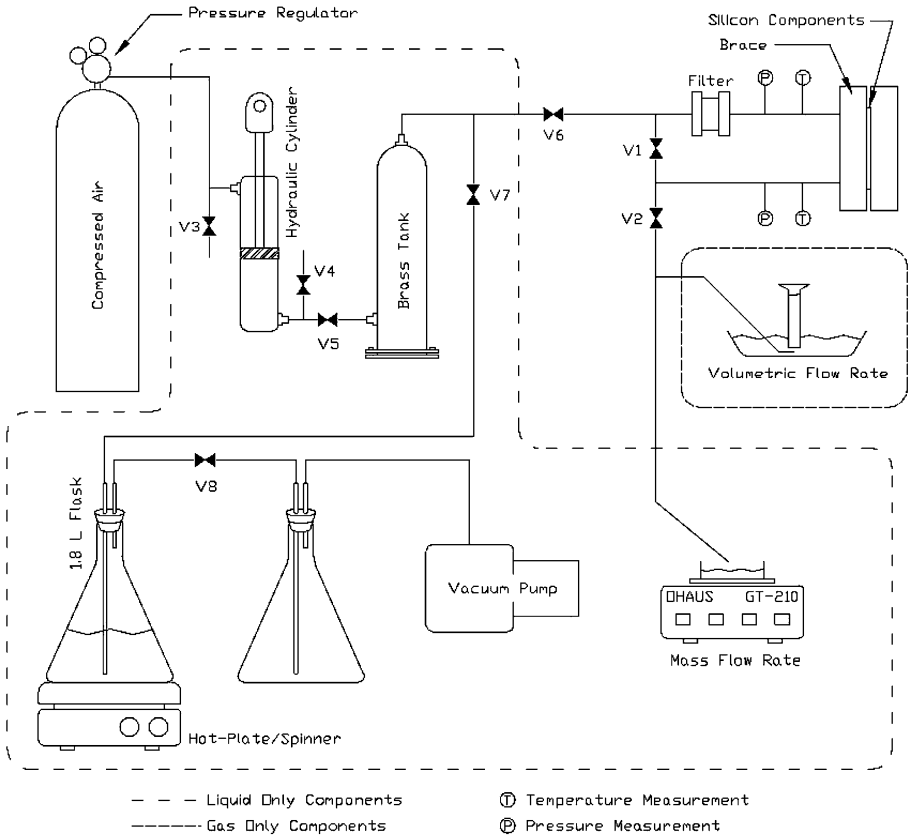

Fig. 5. Schematic of the fluid handling system for the water and gas experiments.

The flow-rate of gas is measured by a volume displacement technique. The gas leaving the experiment is directed into an inverted graduated cylinder filled with water while a digital stopwatch is used to measure the time for the gas to displace the volume of the cylinder. Assuming that the air is an ideal gas,

$$\dot{m} = \frac{V\rho}{\Delta t} = \frac{Vp_v}{(\Delta t)RT_v} \tag{1}$$

where V is the displaced volume, p_v and T_v are the air pressure and temperature in the graduated cylinder, and Δt is the measured time.

During the water experiments, the mass flow-rate is measured by a weighing tank method so that

$$\dot{m} = \frac{m}{\Delta t} \tag{2}$$

where m is the mass of water accumulated over the time period, Δt.

The internal pressure sensors were developed to operate on the principle of the optical lever and utilize an off-chip optical system. The method involves directing a collimated light source at the pressure sensing membrane and observing the change in the reflected angle caused by deformation of the membrane surface. The deflection of the reflected laser is measured by an optical sensor, which is calibrated for pressure measurement.

As shown previously, the silicon chip containing the pressure membranes contains a total of 10 membranes. In order to measure all the membranes a moveable optical system was used. The optical system consists of a laser, lens and a four-quadrant photodiode sensor to measure laser displacement. Fig. 6 shows a simple schematic of the optical setup.

Internal pressure sensor calibration is performed by applying a static pressure to the entire system. The standard pressure transducers in the fluid handling system measure the pressure. The output of the optical system and the standard pressure transducers is measured by the data acquisition system simultaneously. Each calibration is specific to the membrane and the location on the membrane. For all internal pressure measurements, calibration data were obtained twice, once before the internal pressure measurements and once after. This was done to ensure that the calibration had not changed while the system was being used. Uncertainties for the internal pressure calibrations ranged from 1.7% to 13.3% of full scale. Kohl et al. [29,30] describe the internal pressure sensors and the experimental setup in greater detail and include a detailed description of the pressure sensor's accuracy.

2.1. Data reduction

Since experiments of both water and air were performed it was required that the data from each be handled differently. The biggest difference between the two fluids is that the gas flows are compressible and the water flows are incompressible.

For fully developed incompressible fluid flow in a constant cross-sectional channel, the friction factor can be determined from

$$f = \Delta p \frac{D_h}{L} \frac{2}{\rho u^2}. \tag{3}$$

Since the mass flow rate is measured instead of u, it is more convenient to write Eq. (3) in terms of $\dot{m}$ where,

$$\dot{m} = \rho A u, \tag{4}$$

and noting that across the entire channel,

$$\Delta p = p_{c,in} - p_{c,out}, \tag{5}$$

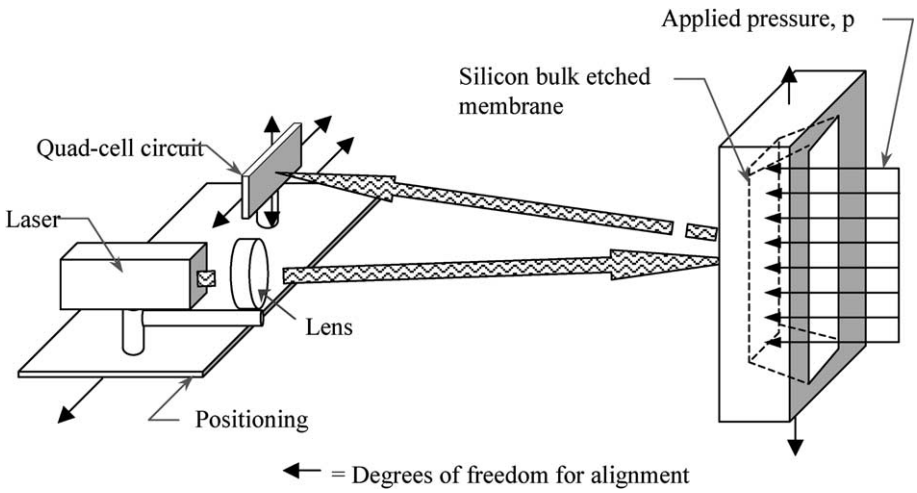

Fig. 6. Schematic of optical positioning system.

Eq. (3) can be rewritten as,

$$f = 2(p_{c,in} - p_{c,out})\frac{D_h}{L}\frac{\rho A^2}{\dot{m}^2}. \quad (6)$$

where $p_{c,in}$ and $p_{c,out}$ are the inlet and exit pressures of the channel, A is the channel cross-sectional area (wh), and D_h is the hydraulic diameter,

$$D_h = \frac{4A}{2w + 2h}. \quad (7)$$

The Reynolds number was calculated from,

$$Re = \frac{D_h \dot{m}}{A\mu}. \quad (8)$$

The Uncertainty B, or range of possible bias, of f and Re were calculated for every data point taken. This Uncertainty B, otherwise called accuracy, was obtained by the standard methods of error propagation analysis. This uncertainty is shown by the error bars in the figures summarizing the results.

When a gas is used as the test fluid, the incompressible assumption is no longer valid and a compressible flow model must be used to determine the friction factor from the measured data. Three nonrestrictive assumptions are made to support this calculation. The cross sectional area and the friction factor are assumed to be constant along the channel, and the channel is taken to be adiabatic. Momentum, mass, and energy balances then give the familiar Fanno flow relation [31] for adiabatic flow with friction,

$$\frac{f(l^* - l)}{D_h} = \frac{1 - M^2}{\gamma M^2} + \frac{\gamma + 1}{2\gamma}\ln\left[\frac{[(\gamma + 1)/2]M^2}{1 + [(\gamma - 1)/2]M^2}\right], \quad (9)$$

where l is the channel length, l^* is the choking length, M is the Mach number and γ is the ratio of specific heats. The adiabatic flow assumption seemed restrictive, so it was compared to an isothermal flow assumption by using a numerical model. It was found that the greatest difference in the friction factor for the two assumptions was on the order of 1%, which is well within the uncertainty of the results of the experiment. The preceding equation is used when the flow is choked at the exit, and the following auxiliary equation is used when the flow is not choked,

$$\frac{f(l_1 - l_2)}{D_h} = \frac{f(l^* - l_2)}{D_h} - \frac{f(l^* - l_1)}{D_h}. \quad (10)$$

Obviously the Mach number is not directly measured in the experiment, so it was eliminated in favor of the measured pressures, temperatures, and mass flux, which are p_1, p_2, T_1, T_2, and ρu. Eqs. (9) and (10) were then combined and further simplified by using the ideal gas equation of state. The resulting equation is,

$$\frac{f(l_1 - l_2)}{D_h} = \frac{p_1^2}{RT_1(\rho u)^2}\left(1 - \frac{p_2^2 T_1}{p_1^2 T_2}\right) + \frac{\gamma + 1}{2\gamma} \times \ln\left[\frac{T_1}{T_2}\frac{2p_2^2\gamma + (\gamma - 1)(\rho u)^2 RT_2}{2p_1^2\gamma + (\gamma - 1)(\rho u)^2 RT_1}\right]. \quad (11)$$

By this procedure the average friction factor between any two points within the channel is determined from Eq. (11) as a function of the variables, p_1, p_2, T_1, T_2, and ρu, and the known ratio of specific heats, γ and ideal gas constant, R.

3. Results and discussion

3.1. Incompressible flow (water) results

In order to determine the average friction factor for the entire channel, the off-chip pressure transducer measurements were used. These measurements were used instead of the internal measurements because of their lower uncertainty and improved repeatability. The disadvantage of using the external pressure measurements is that pressure drops between the pressure transducers and the channel must be accounted for. The benefit of the internal sensors is that the internal pressure measurements validate the assumptions made about the external pressure drop and, while limited in the number of flow rates measured, the internal data will show the variation of pressure along the channel length.

3.1.1. Contribution of other losses

It is necessary to account for the pressure drop between the off-chip pressure transducers and the microchannel before using the pressure transducer data to determine the average friction factor for the microchannel. Minor losses from change in tubing diameter, bends, and tees, were determined by

$$\Delta p = K_L \frac{\rho u^2}{2}, \quad (12)$$

where K_L has been determined previously for various geometries and configurations. Values of K_L can be found in most undergraduate fluid mechanics texts such as Munson et al. [31]. This method was used to obtain the losses inside of the brace, before and after the microchannel. This approach is supported by recent data obtained by Abdelall et al. [32] which show that the loss coefficients associated with single phase flow in sudden area changes in microchannels are comparable to those for large channels with the same area ratios.

Outside of the brace, the pressure loss was determined empirically by connecting the system tubing that would normally connect to the inlet and exit ports of the brace. The pressure drop was measured by the off-chip pressure transducers and was plotted as a function of

the measured mass flow rate. A regression was then made of the external tubing pressure loss as a function of $\dot{m}$ for use in the microchannel data analysis.

Once all losses have been calculated the pressure measurements are corrected in order to represent only the pressure drop inside the channel. The pressure drop is,

$$\Delta p_c = (p_{in} - p_{out}) - \sum \Delta p_{loss,n} - \Delta p_{ext}. \quad (13)$$

This method of determining the minor losses is validated by the internal pressure measurements for each channel. The validation is obtained by plotting the expected pressure drop in the channel that is adjusted for the minor losses and comparing that prediction to the measured internal pressures.

In addition to accounting for the losses outside the channel, it is also necessary to consider the pressure drop associated with developing flow in the entrance region of the channel. Since L/D_h for the channels is as low as 219, it is important to consider the contribution of the entrance region effects. In order to obtain the fully developed friction factor, the pressure drop associated with the developing flow must be subtracted from the pressure drop measured across the entire channel. The method presented by Shah and London [6] is used to determine the pressure drop associated with the developing flow in the entrance region of the channel. The equation used is,

$$\Delta p_{dev} = K_\infty \frac{\rho u^2}{2}, \quad (14)$$

where K_∞ is effectively a loss coefficient associated with the developing flow. K_∞ was measured and calculated by previous researchers and the results were summarized by Shah and London [6].

The pressure drop inside the channel associated with the developing flow was found to be as large as 10% of the measured inlet pressure and as large as 17% of the pressure drop inside channel "e". Clearly it is important to include this effect, especially for the channels with $L/D_h < 300$.

3.1.2. Experimental results for water

The data from channels a, b, d and e with water have been summarized in Fig. 7, which shows all of the data in terms of f_{exp}/f_{th} verses Re. The value of f_{th} was taken to be the analytical, laminar, incompressible values based on Shah and London [6] since no turbulent results were observed. While it would have been desirable to obtain water flow results in the transitional and turbulent regimes, the pressure limitations of the current experimental setup limited the maximum achievable Re for the channel geometries used.

In order to evaluate the amount of scatter of the current data with respect to previous research, Fig. 7 should be compared to Fig. 1. From the two figures it is clear that there is significantly less scatter in the current set of data than for the previous data from other researchers.

The average value of f_{exp}/f_{th} for all of the data in Fig. 7 is 1.04 ± 0.11. The uncertainty of 0.11 is the combined uncertainty, which is computed by combining the Uncertainty B due to possible bias and the Uncertainty A due to scatter or imprecision. The representative Uncertainty B was taken to be the average U_B for all the illustrated data points, which is 0.11. The Uncertainty A for the average was computed by multiplying the sample standard deviation of the illustrated data by the appropriate coverage factor, which is 2.0 in this case. The resulting U_A for the average is very small, so

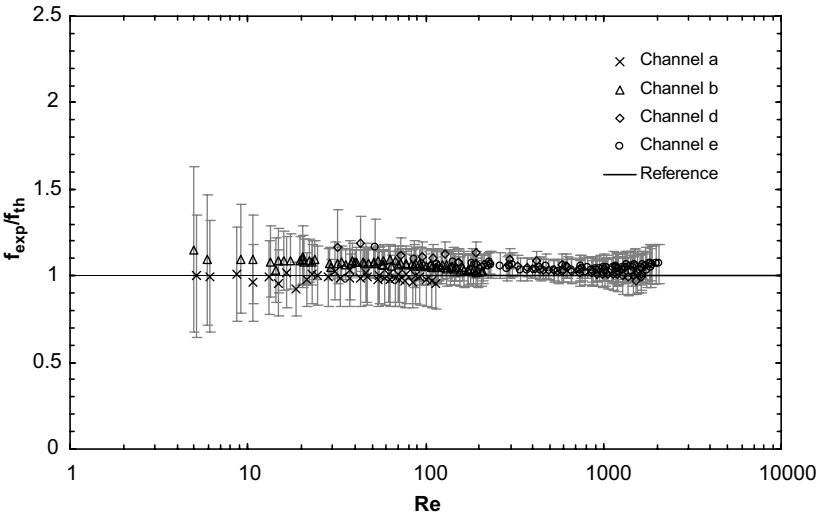

Fig. 7. Comparison of all water data to laminar incompressible flow theory in terms of f_{exp}/f_{th} vs. Re.

the combined uncertainty is very nearly equal to the U_B The difference of 0.04 is small compared to f_{exp}/f_{th} obtained by previous researchers including f_{exp}/f_{th} on the order of 1.3 measured by Wu and Little [11] and f_{exp}/f_{th} on the order of 0.8 measured by Choi et al. [18]. By observing the illustrated U_B of the data in Fig. 7 and from considering the combined uncertainty for the average value, it is clear that the difference between 1.04 ± 0.11 and 1.00 is experimentally insignificant.

From Fig. 7 it is clear that overall agreement between experimental and predicted results is present. Even for the channel with the smallest D_h, excellent agreement between measured and predicted results is shown. Fig. 8 shows the data from channel "a" in terms of fRe versus Re. For the entire range of data taken, the analytical value of fRe for laminar incompressible flow is well within the data uncertainty. Similar results were observed for the other channels as summarized by Fig. 7.

Also illustrated in Fig. 8 is the effect of evaporation from the collection dish during the mass flow rate measurement. One might erroneously assume that the effect of collected water evaporation into the room air would be negligible, however, due to the extremely low mass flow rates through the microchannel this effect becomes significant. Evaporation rates were observed to be as large as 10% of the measure mass flow rate for channel "a". The effect of evaporation is most significant for the lower flow rate tests. By not accounting for evaporation, errors of the measured value of fRe would be as great as 10%. Fig. 8 shows the effect that including the evaporation data has on the final measured values of fRe. The increased uncertainty of fRe at lower Reynolds numbers is due to increases in the percent uncertainty of the pressure measurements at low inlet pressures and the increase in uncertainty of $\dot{m}$ for low mass flow rates.

The data for all channels shows no indication that a transition to turbulence has begun for Re up to 2067. This contradicts the results of previous research including Peng et al. [22] who also tested the flow of water in microchannels and found that transition to turbulence was initiated at $200 < Re < 700$. The present results appear to support the standard findings that laminar flow is maintained for $Re < 2300$.

The early transition to turbulence observed by Peng et al. may have been caused by not properly accounting for the effects of developing flow in the entrance region. Since the analytical values of fRe summarized by Shah and London are for fully developed flow, the additional pressure drop associated with the developing flow in the entrance region should be subtracted from the pressure drop measured across the channel. If the additional developing flow pressure drop is not subtracted from the total pressure drop across the channel, then the effect of developing flow should be included in the theoretical model to which the data is compared. This is done by including the developing flow effect when calculating the pressure drop across the channel,

$$\Delta p = f\frac{L}{D_h}\frac{\rho u^2}{2} + K_\infty \frac{\rho u^2}{2}. \tag{15}$$

Dividing Eq. (15) by $\rho u^2/2$ and multiplying by Re and D_h/L yields the effective value of fRe that includes the modeled effects of the developing flow,

$$(fRe)_{eff} = fRe + K_\infty Re\frac{D_h}{L}. \tag{16}$$

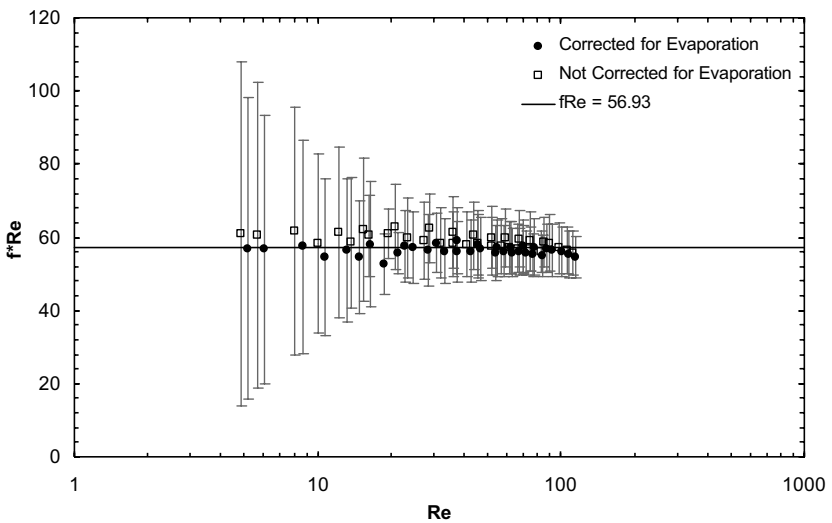

Fig. 8. Friction factor data for water in channel "a" including the effect of evaporation (the analytical prediction of fRe based on Shah and London [6] is 56.93).

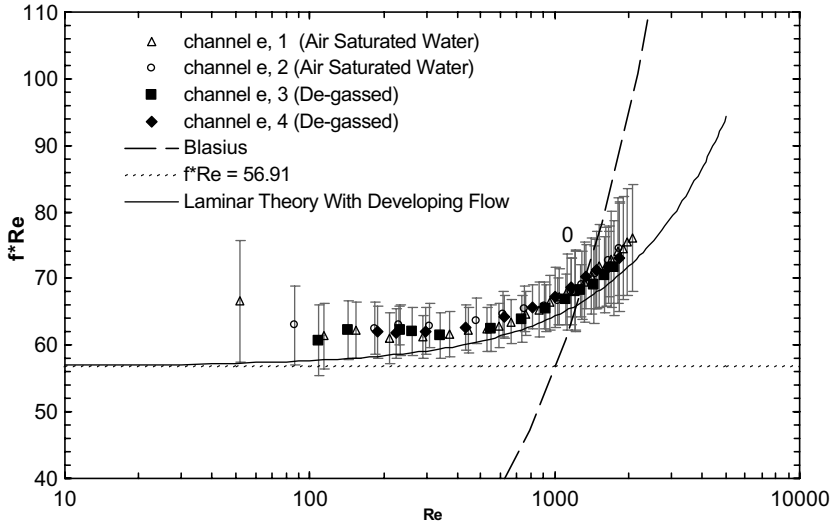

Fig. 9. Friction factor data for water in channel "e" (the analytical prediction of fRe based on Shah and London [6] is 56.91; the solid line is the analytical prediction of Eq. (16) which incorporates the effects of developing flow).

Fig. 9 shows the fRe data for channel "e" and compares it to the prediction of Eq. (16). If the pressure drop associated with the developing flow were not included in the model, the theoretical line for comparison would be a horizontal line at $fRe = 56.91$. When the entrance region effect is not included in the model, the deviation of data from $fRe = 56.91$ could be misinterpreted as a transition to turbulence.

The length-to-hydraulic-diameter ratio, L/D_h, for Peng et al.'s channels varied from 146 to 375. Channel "d" and "e" are both within this range and the data from these channels clearly show how a misinterpretation of the results could lead one to erroneously conclude that an early transition to turbulence, with Re_c is as low as 300, may have taken place.

Fig. 10 shows the internal pressure data for channels "a" and "d". The internal pressure measurements illustrate not only the pressure distribution inside the channel but were also used to validate the entrance and exit loss calculations used to calculate f. Fig. 10 clearly shows the linear variation of pressure along the channel's length that is associated with laminar incompressible flow.

3.2. Compressible flow (air) results

It is typically assumed that the models for incompressible friction factors are also valid for compressible flows. This however is not the case as was shown analytically by Schwartz [33]. He determined that the local friction factor for a compressible fluid inside a channel was dependent on the Mach number, M as well as Re. Since the geometry used in Schwartz's analysis is different from the channels used in these experiments, Shwartz's analytical result could not be used as a theoretical comparison to the measured results of the current experiment. In order to predict f, numerical models of the microchannels were created using the FLUENT computer code [34].

The models used the measured height and width values for the channels. A laminar viscous model was used for all solutions and the viscous heating option was enabled. In order to be consistent with the Fanno flow assumption made in the data reduction method, the walls were assumed to be adiabatic. The air was modeled as an ideal gas with a c_p of 1006.43 J/kg K, thermal conductivity of 0.0242 W/m K, and a viscosity of 1.7894×10^{-5} kg/m s. The effect of grid size was examined to assure validity of the results. The results from the FLUENT numerical model and Schwartz's equation were found to have good agreement in that the friction factor for a given channel predicted by both models increases as the Reynolds number is increased.

It should be noted that the correction for the pressure losses outside the channel and associated with the developing flow in the entrance region of the channel which were important to the water results, were not needed for the gas flows. This is because the pressure losses outside the channel were always less than the uncertainty of the pressure transducers used in the experiment. For the largest Re of channel "e", $\rho u^2/2$ is 1993 Pa (0.3 psi) in the inlet plane of the channel. Since the inlet pressure is 450 psi, the effect of additional inlet and exit losses is negligible.

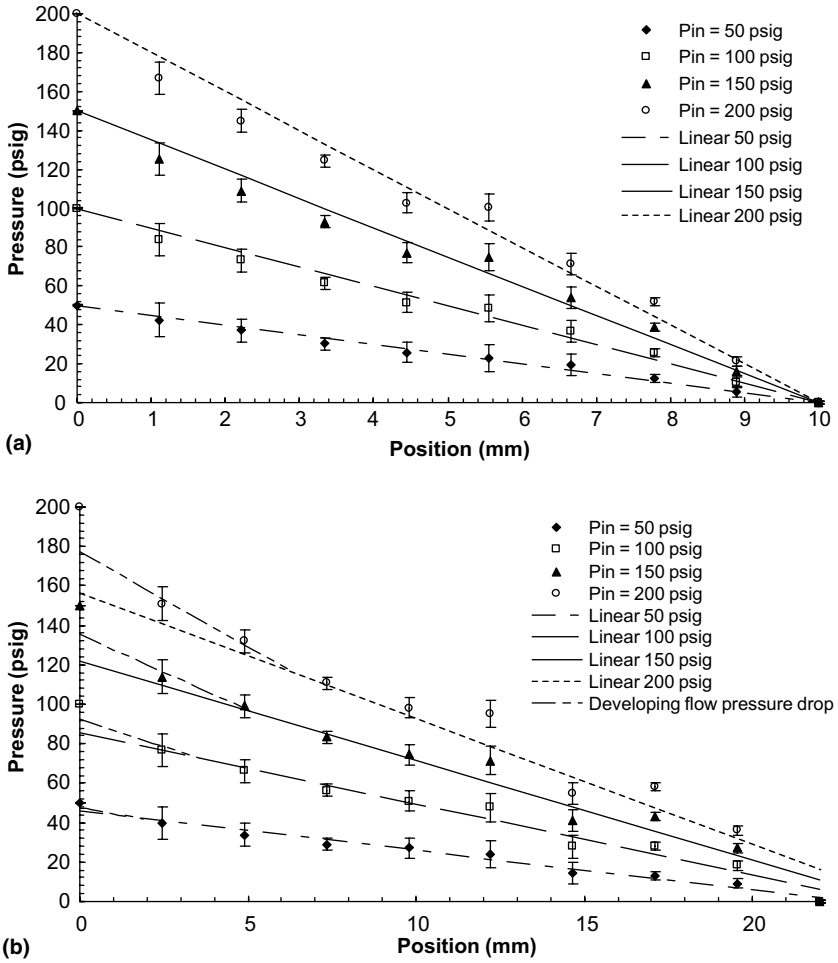

Fig. 10. Internal pressure measurements for water flowing through channel "a" (a) and channel "d" (b). Both cases include the predicted effects of minor losses before and after the microchannel; (b) also includes the predicted pressure drop associated with developing flow.

3.2.1. Compressible experimental results

The compressible flow data from all channels in terms of f_{exp}/f_{th} is plotted as a function of Re in Fig. 11. For $Re < 2300$, f_{th} is the friction factor from the numerical models. For $Re > 2300$, f_{th} is the prediction based on the Blasius equation,

$$f_{th} = 0.316Re^{-1/4}. \quad (17)$$

It should be noted that the Blasius friction factor is not expected to apply for transitional flow ($2300 < Re < 10^4$, shaded part of Fig. 11).

Fig. 11 illustrates good agreement between predicted and measured results. This holds true for all $Re < 2300$ where the flow in all channels is still laminar. Agreement is also illustrated between Blasius and the data for channels "d" and "e" for $Re > 10^4$. Channel "c" also contains a few data points that appear to be turbulent, but has measured values of f that are significantly lower than predicted. While it is tempting to draw conclusions based on the few channel "c" data points with $Re > 10^4$, the Reynolds numbers are too low to eliminate the possibility that the flow is still transitional.

One of the more unexpected observations is the apparent increase in Re_c for some of the channels. This is shown in Fig. 12 where the transition to turbulence appears to occur as late as $Re = 6000$, and in Fig. 13 where $Re > 5300$ is achieved with no indication of a transition to turbulence. This apparent delay of transition to turbulence may be due to the large accelerations in the channel.

In a paper by Kurokawa and Morikawa [35] the effect of acceleration and deceleration on incompressible flows was studied. It was found that increased acceleration of the fluid resulted in an increase of the critical

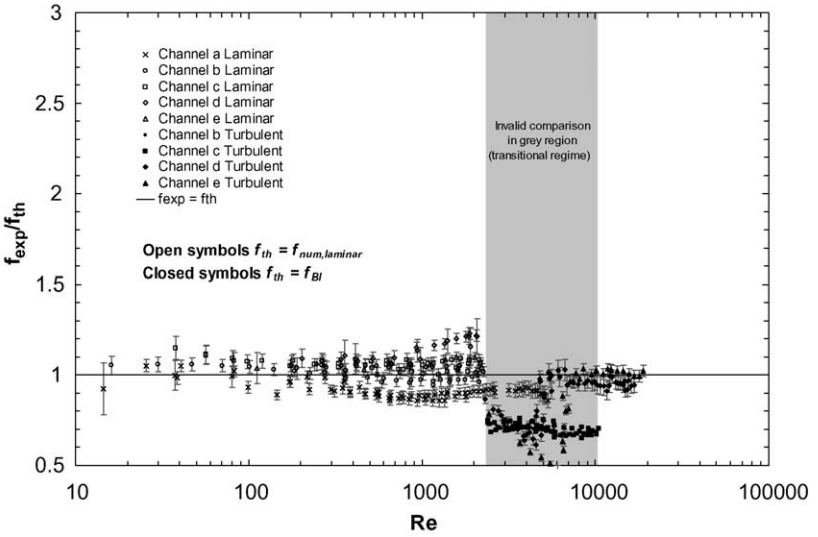

Fig. 11. Comparison of f_{exp} and f_{th} in the form of f_{exp}/f_{th} vs. Re for air.

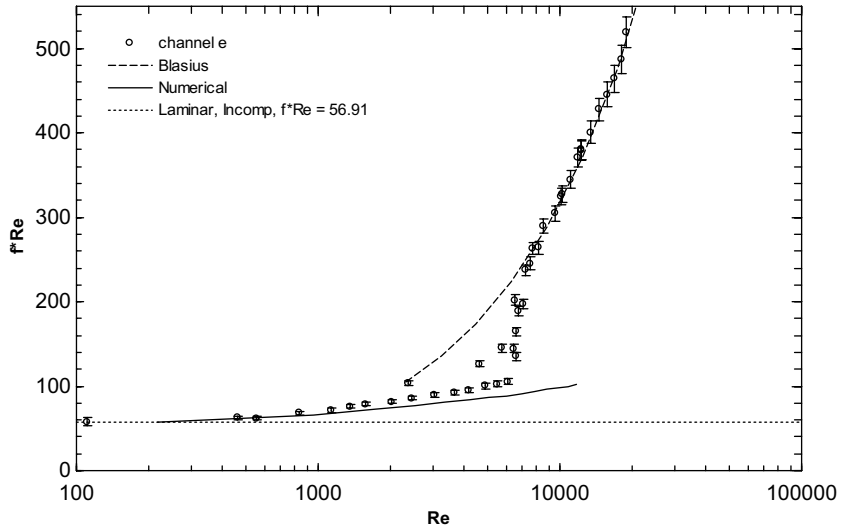

Fig. 12. Friction factor data for channel "e" with air, where 56.91 is the incompressible analytical prediction of fRe based on Shah and London [6] and the solid line is the laminar numerical prediction that accounts for compressibility.

Reynolds number and an increase in the friction factor. Since acceleration is present in the gas microchannels, this may explain the apparent increase in Re_c. Additionally, Kurokawa and Morikawa's observation that acceleration increases f is in general agreement with the results of Schwartz [33] and the present study.

While the increase in Re_c may be explained in terms of the acceleration associated with the compressible flow in the channel, these observations are contrary to the reported observations of previous researchers. None of the present data, both for water and for gas, indicate an early transition to turbulence.

Based on Eq. (9) it is expected that L/D_h is the primary geometric parameter that determines whether compressibility will be significant. Therefore, if the increase in Re_c is related to the compressibility of the flow, the apparent Re_c for each channel should correlate to L/D_h. Fig. 14 plots Re_c as a function of L/D_h. It is clear that as L/D_h is increased, Re_c approaches the standard critical value of $Re_c = 2300$. However, for channels with low L/D_h, Re_c is greater than expected.

These observations conflict with the observations of Wu and Little [11] who reported Re_c as low as 350 for N_2 gas. However, Wu and Little compared their results

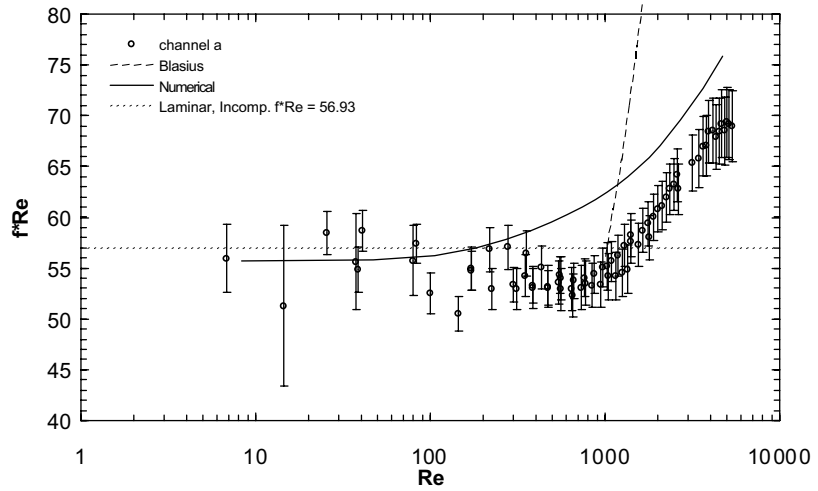

Fig. 13. Friction factor data for channel "a" with air, where 56.93 is the incompressible analytical prediction of fRe based on Shah and London [6] and the solid line is the laminar numerical prediction that accounts for compressibility.

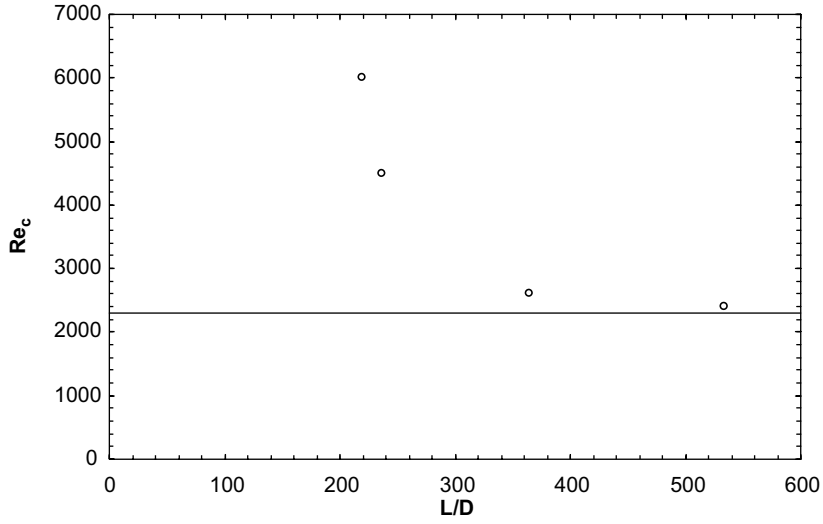

Fig. 14. Re_c for the channels with air as a function of L/D_h.

only to the laminar incompressible prediction, $fRe = 64$ and the Blasius equation. Because of the increase in f due to compressibility, comparison of the measured results to the incompressible laminar flow prediction for f could result in an erroneous identification of Re_c. This may have been the cause of the low Re_c observations by Wu and Little.

Fig. 15 shows some of the internal pressure measurements taken for channel "a" with air. The solid lines in the figure come from the numerical model of channel "a" and includes the effects of compressibility. The variation of the pressure gradient due to the flow compressibility should be noted. The measured pressure distributions show good agreement with the numerical predictions, reinforcing the importance of compressibility and highlighting the potential for error when applying incompressible flow models to gaseous microchannel flows.

4. Conclusions

The goal of this investigation has been to measure the pressure drop in microchannels in an attempt to determine the sources of unusual and often conflicting results previously reported in the literature. Microfabrication

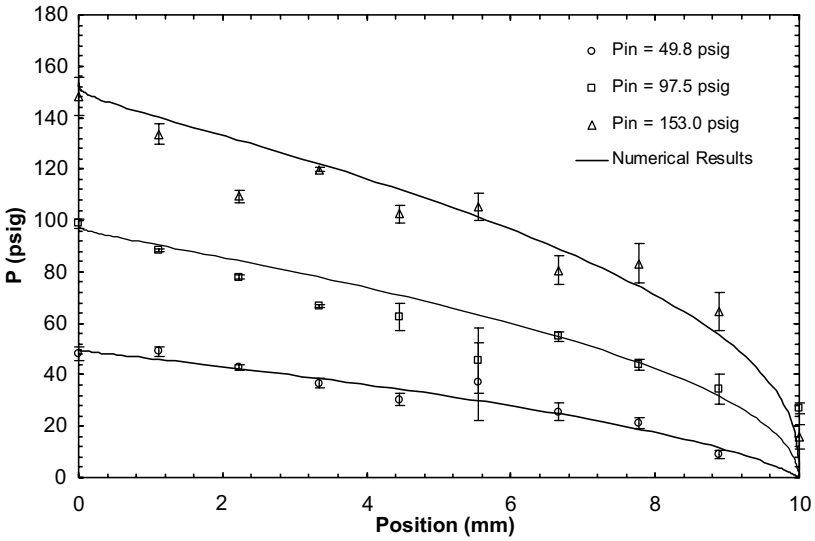

Fig. 15. Internal pressure measurements for channel "a" with air.

techniques were used to design and build microchannel test sections that incorporate internal pressure measurements. The internal pressure measurements provide information about the pressure drop inside the channel and provide validation for the methods used to determine average channel friction factors.

4.1. Incompressible microchannel flow

The present investigation shows agreement between standard laminar incompressible flow predictions and measured results for water. Based on these observations the predictions based on the analytical results of Shah and London [6] can be used to predict pressure drop for water in channels with D_h as small as 24.9 μm.

These results differ from the conclusions of several individual researchers. However, when all of the data from different researchers is taken together, the data appears to be scattered both above and below the analytical predictions. It is believed that the consistent offsets observed by individual researchers is the result of unaccounted for bias in experimental setups, such as over or under estimating pressure drops outside of the channel or not accounting for increased pressure drop in the entrance region of the channel. These problems were largely avoided in the present study by using the internal pressure measurements to validate the external pressure loss models used. The present results highlight the importance of accounting for common phenomena that are often negligible for standard flows such as accounting for evaporation during the mass flow rate measurements.

Peng et al. [22] is widely referenced for observing an early transition to turbulence for the flow of water in microchannels. The present study has found no such evidence of early transition for the channel dimensions and range of *Re* tested, including *Re* up to 2067. It is believed that one reason for the observation of low Re_c in previous studies was that channels with relatively low L/D_h were used and the effects of increased pressure drop in the entrance region of the channel was unaccounted for.

4.2. Compressible microchannel flow

The present investigation has shown that it is insufficient to assume that *f* for laminar compressible flow can be determined using the well-known analytical predictions for laminar incompressible flow. In fact, experimental and numerical results both show that *f* increases beyond f_{inc} as *Re* is increased for a given channel with air. In contrast, a standard numerical simulation that considers compressibility and entrance effects does agree well with our data.

In order to accurately predict *f* for compressible flows one may be able to use the analytical results from Schwartz [33] as an initial approximation. In order to more accurately predict *f* one could use a numerical model as was done in this investigation. A more detailed investigation of the compressibility effect on *f*, resulting in an improved correlation or analytical prediction would be very beneficial to gas microchannel flows.

In addition to influencing *f*, experimental results indicate that compressibility can increase the apparent Re_c beyond the standard value of 2300. This is likely caused by the large accelerations present in the channels. It has also been shown that Re_c may be related to L/D_h where lower values of L/D_h tend to increase Re_c. These observations are different from the observations of Wu and

Little [11] who reported Re_c as low as 350 for nitrogen gas. However, Wu and Little compared their results only to the laminar incompressible prediction, $fRe = 64$ and the Blasius equation. As was shown by the current results, comparison of the measured results to the incompressible laminar flow prediction for f could result in an erroneous identification of Re_c. This may have been the cause of the low Re_c observations by Wu and Little.

References

[1] D.B. Tuckerman, R.F. Pease, High-performance heat sinking for VLSI, IEEE Electron Dev. Lett. 2 (5) (1981) 126–129.

[2] P. Wilding, M.A. Shoffner, L.J. Kircka, Manipulation and flow of biological fluids in straight channels micromachined in silicon, Clin. Chem. 40 (1994) 43–47.

[3] I. Papautsky, B.K. Gale, S. Mohanty, T.A. Ameel, A.B. Frazier, Effects of rectangular microchannel aspect ratio on laminar friction constant, SPIE 3877 (1999) 147–158.

[4] X.N. Jiang, J.Y. Zhou, Y.L. Yao, X.Y. Ye, Micro-fluid flow in microchannel, Proc. Transducers 95 (1995) 317–320.

[5] G.M. Mala, D. Li, Flow characteristics of water in microtubes, Int. J. Heat Fluid Flow 20 (1999) 142–148.

[6] R.K. Shah, A.L. London, Laminar Flow Forced Convection in Ducts, Academic Press, New York, 1978.

[7] Q. Weilin, G.M. Mala, L. Dongqing, Pressure-driven water flows in trapezoidal silicon microchannels, Int. J. Heat Mass Transfer 43 (2000) 353–364.

[8] H.Y. Wu, P. Cheng, Friction factors in smooth trapezoidal silicon microchannels with different aspect ratios, Int. J. Heat Mass Transfer 46 (2003) 2519–2525.

[9] H.B. Ma, G.P. Peterson, Laminar friction factor in microscale ducts of irregular cross section, Microscale Thermophys. Eng. 1 (1997) 253–265.

[10] K.V. Sharp, R.J. Adrian, Transition from laminar to turbulent flow in liquid filled microtubes, Exper. Fluids 36 (2004) 741–747.

[11] P. Wu, W.A. Little, Measurement of friction factors for the flow of gases in very fine channels used for microminiature Joule–Thompson refrigerators, Cryogenics 23 (1983) 273–277.

[12] H. Blasius, Forschungsarbeiten des Ver. Deutsh. Ing., p. 131.

[13] J. Pfahler, J. Harley, H. Bau, J. Zemel, Liquid transport in micron and submicron channels, Sensors Actuat. A21–A23 (1991) 431–434.

[14] J. Pfahler, J. Harley, H. Bau, J. Zemel, Gas and liquid flow in small channels, Micromech. Sensors Actuat. Syst. 32 (1991) 49–60.

[15] J.C. Harley, Y. Huang, H.H. Bau, J.N. Zemel, Gas flow in micro-channels, J. Fluid Mech. 284 (1995) 257–274.

[16] P.M.-Y. Chung, M. Kawaji, A. Kawahara, Characteristics of single-phase flow in microchannels, ASME Fluids Eng. Div. Publ. FED 257 (1B) (2002) 1219–1227.

[17] E.B. Arkilic, M.A. Schmidt, K.S. Breuer, Gaseous slip flow in long microchannels, J. Microelectromech. Syst. 6 (1997) 167–178.

[18] S.B. Choi, R.F. Barron, R.O. Warrington, Fluid flow and heat transfer in microtubes, Micromech. Sensors Actuat. Syst. 32 (1991) 123–134.

[19] F.W. Dittus, L.M. Boelter, Heat transfer in automobile radiators of the tubular type, Univ. Calif. Berkeley Publ. Eng. 2 (13) (1930) 443–461.

[20] D. Yu, R. Warrington, R. Barron, T. Ameel, An experimental and theoretical investigation of fluid flow and heat transfer in microtubes, ASME/JSME Thermal Eng. Conf. 1 (1995) 523–530.

[21] H.E. Hegab, A. Bari, T. Ameel, Friction and convection studies of R-134a in microchannels within the transition and turbulent flow regimes, Exper. Heat Transfer 15 (2002) 245–259.

[22] X.F. Peng, G.P. Peterson, B.X. Wang, Frictional flow characteristics of water flowing through rectangular microchannels, Exper. Heat Transfer 7 (1994) 249–264.

[23] X.F. Peng, G.P. Peterson, B.X. Wang, Heat transfer characteristics of water flowing through microchannels, Exper. Heat Transfer 7 (1994) 265–283.

[24] X.F. Peng, B.X. Wang, Forced-convection and boiling characteristics in microchannels, in: Proceedings of the 11th IHTC 1, 1998, pp. 371–390.

[25] K.-C. Pong, C.-M. Ho, J. Liu, Y.-C. Tai, Non-linear pressure distribution in uniform microchannels, ASME Appl. Microfabric. Fluid Mech. FED-197 (1994) 51–56.

[26] J.C. Shih, C.-M. Ho, J. Liu, Y.-C. Tai, Monatomic and polyatomic gas flow through uniform microchannels, Microelctromech. Syst. (MEMS) DSC 59 (1996) 197–203.

[27] X. Li, W.Y. Lee, M. Wong, Y. Zohar, Gas flow in constriction microdevices, Sensors Actuat. A 83 (2000) 277–283.

[28] D. Pfund, D. Rector, A. Shekarriz, A. Popescu, J. Welty, Pressure drop measurements in a microchannel, AIChE J. 46 (2000) 1496–1507.

[29] M.J. Kohl, S.I. Abdel-Khalik, S.M. Jeter, D.L. Sadowski, A microfluidic experimental platform with internal pressure measurements, Sensors Actuat. A, in press.

[30] M.J. Kohl, An experimental investigation of microchannel flow with internal pressure measurements, Ph.D. thesis, Georgia Institute of Technology, May 2004.

[31] B.R. Munson, D.F. Young, T.H. Okiishi, Fundamentals of Fluid Mechanics, John Wiley and Sons, Inc., New York, 1990.

[32] F. Abdelall, G. Hahn, S.M. Ghiaasiaan, S.I. Abdel-Khalik, S.M. Jeter, M. Yoda, D. Sadowski, Pressure drop caused by abrupt flow area changes in small channels, Exper. Thermal Fluid Sci., in press.

[33] L.W. Schwartz, A perturbation solution for compressible viscous channel flows, J. Eng. Math. 21 (1987) 69–86.

[34] FLUENT 6.0 Documentation, 2001.

[35] J. Kurokawa, M. Morikawa, Accelerated and decelerated flows in a circular pipe (1st report, velocity profile and friction coefficient), Bull. JSME 29 (1986) 758–765.